Journal of Materials Chemistry C

Accepted Manuscript

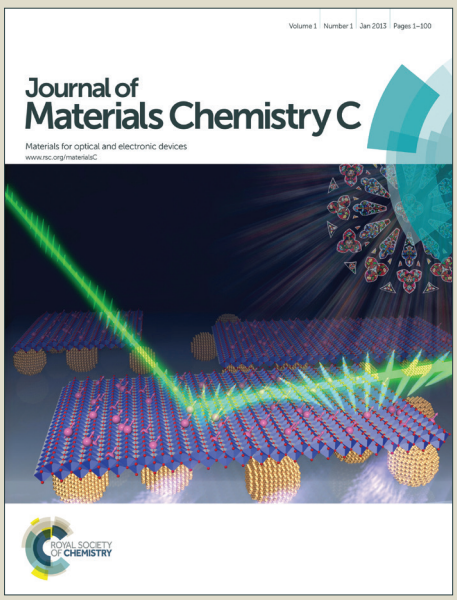

ROYAL SOCIETY OF CHEMISTRY

www.rsc.org/materialsC

Journal Name

RSCPublishing

COMMUNICATION

An isoindigo containing donor-acceptor polymer: synthesis and photovoltaic properties of all-solution-processed ITO- and vacuum-free large area roll-coated single junction and tandem solar cells

Cite this: DOI: 10.1039/x0xx00000x

Received 00th January 2012,
Accepted 00th January 2012

DOI: 10.1039/x0xx00000x

www.rsc.org/

Rasmus Guldbaek Brandt [a,b,†], Wei Yue [a,b,†], Thomas Rieks Andersen [c], Thue Trofod Larsen-Olsen [c], Mogens Hinge [d], Eva Bundgaard [c], Frederik C. Krebs [c], Donghong Yu [a,*]

In this work, the design, synthesis, and characterization of a donor-acceptor polymer from dithieno[3,2-b:2',3'-d]pyrrole and isoindigo (*i*-ID) are presented. The synthesized polymer has been applied in large area ITO-free organic photovoltaics, both as spin coated and roll coated devices; the latter as both single junction and multi junction organic photovoltaic (OPV) architectures.

In recent years, for organic photovoltaics (OPVs) there has been an increasing focus on development of electron deficient heteroaromatic moieties in donor-acceptor (D-A) type conjugated polymers, such as phthalimide (PI)[1], naphthalene diimide (NDI)[2], perylenediimide (PDI)[3], benzothiadiazole (BT) and benzobis(thiadiazole) (BBT) [4], diketopyrrolopyrrole (DPP)[5], benzodipyrrolidone (BDP)[6] and thieno[3,4-c]pyrrole-4,6-dione (TPD)[7], and isoindigo (*i*-ID)[8]. When incorporated with donor units (alternating) in the polymer backbone, this electron richness and electron deficiency ensures a low band gap, thus allowing for more efficient absorbance of the incident solar photons over a wider part of the solar spectrum.[9]

Electron deficient monomers are essential to the design of low band gap (LBG) conjugated polymers, as such moieties in the polymer main chain exhibit high electron affinity and strong ability to reduce the band gaps of D-A polymers compared to the corresponding homo-polymers. They can especially tune the energy level of the lowest unoccupied molecular orbital (LUMO) of the given polymer, which is the key parameter; being associated with charge transfer process in OPVs. The optimal driving force for the charge transfer process has been commonly recognized as 0.3 eV, i.e. the LUMO energy difference between the donor (such as D-A polymer) and the acceptor (state-of-art phenyl-C61-butyric acid methyl ester (PC[60]BM))[10]. Among these previously mentioned acceptor moieties, *i*-ID is especially interesting as an efficient acceptor block; due to its strong electron-withdrawing characteristics and a large optical transition dipole, the interest was firstly sparked by Reynolds *et al*.[11] that showed an *i*-ID containing oligothiophene as a p-type OPV material, with a power conversion efficiency (PCE) of 1.76%. Soon after independent reports followed since 2011; by Zhang *et al.*[12] Liu *et al*.[13], and Wang *et al*.[14] with PCE ranging from 1 to 3 %, the high PCE of 6.3% was obtained by Wang *et al*.[15] in 2011. This was until very recently the best performing *i*-ID containing polymer, but it was overtaken by Geng *et al*.[16] who reported a PCE of 8.2% in 2014, which is now the highest PCE of *i*-ID based LBG polymers. In the meantime, for D-A LBG conjugated polymers, the fused ring donor unit dithieno[3,2-b:2',3'-d]pyrrole (DTP) is a widely used electron rich moiety and has been proven to have excellent electron donating properties and good molecular planarity. Similar D-A combination of bisthiophene-DTP (BT-DTP) has been reported by Wu *et al.* poly(bisthiophenedithieno[3,2-b:2',3'-d]pyrrole-isoindigo)(PBTDTPI) afforded OPV with efficiencies in the range of around 1.86 %[17]. However, all above-mentioned "hero" *i*-ID based LBG polymer solar cells including **PBTDTPI** are single junction solar cells with small active areas (not exceeding 0.1 cm^2) on rigid glass substrates using ITO as semitransparent front electrode and vacuum evaporated metal back electrodes. Indium scarcity, its high market demand and the high energy input required in ITO production using vacuum techniques; have become the bottleneck in developing/commercializing OPVs due to the resulting non-sustainability, high cost and high energy payback time[18]. Therefore the replacement of indium becomes essential and the substitute should preferably be a solution-based ambient processable system. A possible combination of Poly(3,4-ethylenedioxythiophene) Polystyrene sulfonate(PEDOT:PSS) with a metal grid remaining on flexible plastic (e.g. PET) substrates turns to be most readily scalable, facile alternative to ITO coated glass[18]. Large area ITO- and vacuum-free OPVs fabrication in a fast and scalable manner is the roll-to-roll (R2R) slot-die coating, which has been identified and explored as a large array of techniques by few groups; but with great successes so far. However, all but a few reports have used poly(3-hexylthiophene) (**P3HT**) as polymer donor[19]. Although above-

introduced *i*-ID containing D-A LBG polymers have outperformed **P3HT** in regards to PV performance with PCEs up to 7.2%, there is no guarantee on transferring this high PV performance when upscaled to a R2R setting from conventional spin-coating and vacuum deposition techniques. It is due to the inherent differences in processing, many of the achievements for small area OPVs are likely to prove difficult to reproduce using the R2R methods. In order to minimize/close this gap of knowledge, more efforts must be put on the testing of new promising materials in R2R fabricated PSCs. As a consequence of the discrete nature of the absorbance bands of conjugated organic molecules, a necessity to absorb different regions of the solar spectrum emerges. To capture the entirety of the solar spectrum, tandem solar cells with compensated light absorption can be employed. Such tandem structure will in principle lead to a higher performance than the single junction in spite of the expense of extra processing steps and enhanced material consumptions. In this paper, a novel D-A polymer **PDTPI** incorporating DTP and *i*-ID as donor and acceptor moieties, respectively, was successfully synthesized via Pd-catalyzed Stille coupling reaction. Vacuum- and ITO-free OPVs from **PDTPI** has been roll-coated as single junction and tandem solar cells with **P3HT** and **PBDTTTz-4** in the area scale of 1 cm^2, and the photophysical and electrochemical properties of **PDTPI**, and photovoltaic properties of spincoated single junction and roll coated large area (~1 cm^2) single junction and tandem cells were fully investigated.

Experimental

Materials and synthesis. The monomers 2,6-di(trimethyltin)-*N*-(1-pentylhexyl)dithieno[3,2-*b*:2',3'-*d*]-pyrrole and 6,6'-dibromodi(2-ethylhexyl)isoindigo was synthesized following procedures reported in literature[11,20]. Poly-3-hexylthiophene (P3HT from Plextronics) had a M_n of 40.000 Da. PBDTTTz-4 were synthesized according to literature procedures[37,38], Phenyl-C_{61}-butyric acid methyl ester (PC[60]BM, from Solenne) had a purity of 99%. PEDOT:PSS was purchased from Agfa (Orgacon EL-P 5010), or Heraeus (Clevious P VP Al 4083, and Clevious F-010). Electron transport layers (ETL) were coated using a stabilized ZnO nanoparticle solution in acetone. Thermally curable Ag (PV-410) was purchased from Dupont. All other chemicals were used as received, unless noted.

Polymerization of PDTPI. A mixture of 2,6-di(trimethyltin)-*N*-(1-pentylhexyl)dithieno[3,2-*b*:2',3'-*d*]-pyrrole (104.30 mg, 0.158 mmol), 6,6'-dibromodi(2-ethylhexyl)isoindigo (100.00 mg, 0.155 mmol), tris(dibenzylideneacetone)dipalladium $Pd_2(dba)_3$, 2.84 mg, 3.10 µmol), and tri-o-tolylphosphine ($P(o\text{-}Tol)_3$, 7.55 mg, 24.8 µmol) was preliminarily degassed with N_2, and then toluene (16 mL) was added. The mixture was further purged with N_2 for 20 min and heated to 120 ^oC for 48 hr. Subsequently the reaction was cooled to room temperature and the solution was precipitated in methanol. The crude polymer was collected by filtration and then purified on a soxhlet's extractor with using acetone and hexane in succession. The polymer was extracted with chloroform and obtained by precipitating the chloroform solution in methanol. Yielding 105 mg (55 %) solid dark polymer. GPC: 8860 Da; PDI 1.52. ^1H NMR (600 MHz, $CDCl_3$, δ, ppm): 9.11 (d, 2 H), 6.65-7.31 (m, 6 H), 4.39 (s, br, 1 H), 3.75 (s, br, 4 H), 0.95-2.27 (m, br, 52 H).

Measurements. ^1H NMR spectra were recorded on a Bruker AvanceIII 600 MHz spectrometer. High temperature gel permeation chromatography (HT-GPC) measurements were conducted on PL-GPC220 equipment at 150 ^oC with 1,2,4-trichlorobenzene as eluent and polystyrene as standards. Thermogravimetric analysis (TGA) was carried out on a PerkinElmer STA6000 simultaneous thermal analyzer at a heating rate of 10 °C min^{-1} under nitrogen flow. UV-vis absorption was recorded on a Varian 50 Bio UV-vis spectrophotometer. Cyclic voltammetry (CV) was performed on a CHI660B electrochemical analyzer (CH Instruments) using a three-electrode cell set up with 0.1 M $TATBF_4$ in acetonitrile as electrolyte at a scan rate of 1 $V \cdot s^{-1}$. A glassy carbon working electrode with a diameter of 1 mm, a platinum-counter electrode, and Ag/Ag^+ phedo reference electrode was applied. The potential was calibrated against the ferrocene/ferrocenium redox couple (Fc/Fc^+, 4.8 eV below the vacuum level). The highest occupied molecular orbital (HOMO) and the lowest unoccupied molecular orbital (LUMO) were estimated by the equations: HOMO = - (4.80 + E_{ox}^{onset}) and LUMO = HOMO+ $E_{bg}^{optical}$.

Solar Cells Fabrication and Characterization

Spin-coated single junction solar cell. Single junction devices were prepared on a flexible poly(ethylene terephthalate) (PET)substrate using a highly conductive PEDOT:PSS (Heraeus Clevious PH1000) for charge collection, the electron transport layer (ETL) were spin-coated using an aluminium doped ZnO nanoparticle solution in acetone (49 mg/mL) at 1000 rpm followed by spin coating of a dichlorobenzene solution of **PDTPI**:PC[60]BM (1:2, 20 mg/mL) at 600 rpm. The hole transport layer (HTL) of PEDOT:PSS (Agfa EL-P-5010:Isopropanol 2:1 w/w) was spin-coated at 3000 rpm, and finally Ag was vacuum evaporated as the back electrode (Ag). The active area of the OPV cell was 0.25 cm^2.

Roll-coated single junction solar cell. All roll coated devices were printed on a substrate known as Flextrode comprising PEDOT:PSS (Heraeus Clevious PH1000) and ZnO on barrier material with a large scale roll-to-roll flexographic printed silver grid electrode. The active layer **PDTPI**:PC[60]BM (1:X), HTL PEDOT:PSS (Clevious P VP Al 4083 and Clevious F-010) were all slot-die coated as detailed reported by Andersen *et al*.[21,22] The back silver electrode was applied by flexographic printing of a heat curing silver paste PV410 (Dupont) as previously reported[22]. All cells possess an active area of 1 cm^2. All layer thicknesses can be seen in ESI **Table S1**.

Roll-coated tandem solar cell. Tandem cells were coated in a comparable method that applied on roll-coated single junction solar cells as described above. LBG polymers **PBDTTTz-4**: PC[60]BM (1:1) and **PDTPI**:PC[60]BM (1:2) were slot-die coated as the first and second active layers, respectively, isolated by PEDOT:PSS F010, Al 4083 and ZnO layers in between. To minimize the risk of solvent penetration through the intermediate layer the second active

layer was coated at 60 °C for faster evaporation. Prior to flexorgraphic printing of silver electrode, three PEDOT:PSS layers namely F010, 4083 and F010 (seen above) were employed by slot-die coating. Detailed printing processes were described by Andersen *et al*.[21,22] All layer thicknesses can be found in ESI **Table S2**.

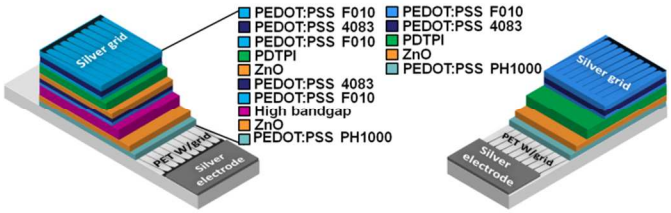

Figure 1. Schematic structure of slot-die coated tandem solar cell (left) and single junction solar cell (right)

Solar cell performance. Solar cells were measured with a Keithley 2400 sourcemeter under a KHS 575 solar simulator with an AM1.5G 1000 W/m^2 intensity. The external quantum efficiency (EQE) was performed using a QEX10 system (PV Measurements).

Results and Discussion

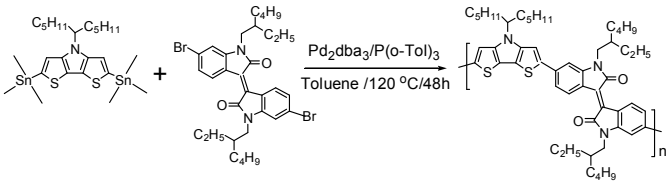

Scheme 1. Stille cross-coupling of 2,6-di(trimethyltin)-*N*-(1-pentylhexyl) dithieno[3,2-*b*:2',3'-*d*]-pyrrole and 6,6'-dibromodi(2-ethylhexyl)isoindigo to affording the polymer PDTPI.

Synthesis. The structures and synthetic route to the polymer PDTPI is illustrated in **Scheme 1**. **PDTPI** were synthesized via Stille cross-coupling reaction between 2,6-di(trimethyltin)-*N*-(1-pentylhexyl)dithieno[3,2-*b*:2',3'-*d*]-pyrrole and 6,6'-dibromodi(2-ethylhexyl)isoindigo that were prepared according to literature procedure respectively[11,20], resulting in a reasonable reaction yield of 55%. The obtained polymer had a relatively low M_n of 8,860 g/mol resulting from poor solubility of **PDTPI** in toluene. The thermal decomposition temperature (5% mass loss) was found to be 388°C (see ESI **Fig. S1**), proving a sufficient thermal stability for device fabrication and application.

Photophysical properties. Fig. 2 presents the UV-vis absorption spectrum of **PDTPI** acquired in both chloroform solution and thin film. Compared to the weak absorption for π-π* transition in the high energy band ranging 300-500 nm, the intense absorption in the low-energy band range of 550-900 nm evident strong electron-withdrawing effect of *i*-ID moiety and the intramolecular charge transfer (ICT) between DTP and *i*-ID entities. As depicted, the maximum absorption bands of **PDTPI** in solution were reached at 400 and 820 nm, while in film they were unusually blue-shifted to 390 and 790 nm. We suppose that such blue shifts in absorption of polymer films may originate from two possible aspects: a) the aggregation of the polymer chains formed in solution; or b) the presence of two branched alkyl chains on both the D and A moiety, in particular on the *i*-ID unit has a larger effect on the spatial arrangement of the copolymers to retard the intermolecular π-π interactions, therefore weak π-π stacking could be assumed. For the former, that has been reported in our previously published work that blue shifts of 5-19 nm from solution to film absorption on D-A LBG polymers comprising dithieno[3,2-*b*:2',3'-*d*]pyrrole as donor unit and phthalimide or thieno[3,4-c]pyrrole-4,6-dione as acceptor[20]. That had been furthermore proved by a blue-shift of 5-13 nm in chlorobenzene (CB) solution absorption of the same polymers at 70 °C, compared to those measured 25 °C also in CB. Such blue shifts in solution could be attributed to breakup of interchain aggregates in solution at the elevated temperature[23,24] also as suggested by another report on poly-benzodipyrrolidone and dithieno[3,2-*b*:2',3'-*d*]pyrrole[6]. For the latter, as reported by Su *et al.*, existence of aliphatic segments on poly(cyclopenadithiophene-alt-isoindigo) in form of both long linear- and short branched-side chains on either donor or acceptor units has proven the same blue-shift of low-energy band absorption from solution to films[25].Stalder *et al.* observed similar phenomena on *i*-ID and dithieno[3,2-b:2',3'-d]silole copolymer pronounced a slight blue shift of about 5 nm from its solution absorption to that in films[26]. Meanwhile, the broader ICT band in film than that in solution implies strong and more efficient charge transfer formed in the solid state facilitating charge transport. The optical band gap ($E_{bg}^{optical}$), according to the equation $E_{bg}^{optical} = 1240/\lambda_{edge}$, was calculated to be 1.38 eV.

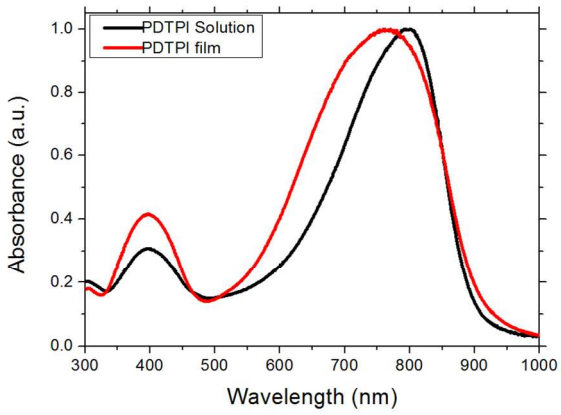

Figure 2. UV-vis spectra of PDTPI in chlorobenzene solution (black line) and film (red line)

Molecular modelling. Density functional theory (DFT) was used to investigate the optimal geometric structure and the electronic configuration of **PDTPI**, this was done at the B3LYP/6-31G(d) level using Gaussian 09 and visualized with GaussView 5.0.9. To reduce the computational load, the aliphatic side-chains are reduced to methyl groups, as this has been shown in literature not

to affect the frontier orbital, while affecting the torsion angle to some extent[26]. As the system investigated was a polymer; two different methods of evaluation was setup. The first being simply one repetition of a donor unit and an acceptor unit, and the other was 3 consecutive donor acceptor units, thereby simulating the rather extended conjugation of polymers. Salvatori *et al*.[27] showed that this trimer setup gives decent results when simulating a similar system. The orbitals that are interesting in DFT modelling are the frontal orbitals i.e. the HOMO and LUMO. The geometrically optimized structure of both the single D-A and the three repeating D-A moieties is shown in **Fig. 3.** The dihedral angle between the single D-A model is 21.99°, and the 3 repeating D-A moieties all show similar angles ranging from 20.87 to -20.45° as seen in ESI **Fig. S3**.

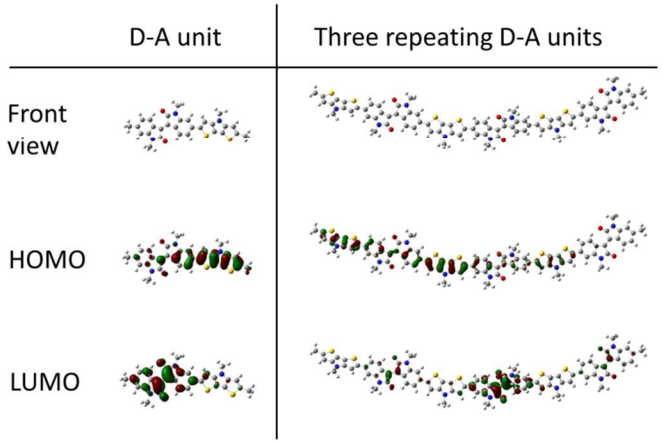

Figure 3. DFT modelling at the B3LYP/6-31G(d) level by gaussian 9 of donor-acceptor model compound and for three consecutive D-A configureations.

This continues twist will afford a torsion on the backbone, thus explaining why there is practically no difference between the absorption of the film and the solution with less than 25 nm onset redshift[28]. The modelled torsion angle corresponds to the findings of Lei *et al*.[29] and Wang *et al*.[30] with angles similar to the modelling results, likewise this affords a small red shift onset of the solid state absorbance. While Wang *et al*. argues that the small change/redshift of the absorbance onset is ascribed to tight aggregation of the polymers in solution; in the case of **PDTPI** having this continues torsion this is seemingly also the case. Wang *et al.* also model a fluorinated *i*-ID moiety, which afford very small torsion angle between the donor and the acceptor moiety (~0.01°), following the argument of the solvated polymeric interaction (π-stacking) should be significantly increased thus expecting a large red shift, which is not observed, indicating that even though the torsion angles are continues, the angles are negligible and thus have a low effect on the π-stacking in both film and in solution. Due to the simplifications of the DFT model with regard to the side-chains which has also been shown to influence the torsion angle[27], whilst this is true the tendencies are still valid.

From the single D-A model, it is clear that the HOMO is primarily located on the donor moiety (DTP) and the LUMO is likewise located mainly on the (*i*-ID) moiety, as expected. This is also supported by the clear intermolecular charge transfer seen in the absorbance spectra, as described earlier.

The predicted HOMO and LUMO levels are -4.80 eV and -2.52 eV giving a band gap of 2.28 eV. This band gap differs from the experimentally determined levels, which is much lower (as the onset of absorbance is approximately 898 nm (**Fig. 2**)). The 3 repeating D-A units, show the same tendencies with only a slight change in the predicted HOMO level given at -4.77 eV while the LUMO level is -2.69 eV. The computed band gap of the 3 repeating D-A units is 2.08 eV which still deviates from the experimental values. The modelling falls in line with the findings of Zhaung *et al*.[31] who found that the frontier orbital of LUMO and HOMO, of a donor-acceptor polymer, was primarily attributed to the acceptor and donor, respectively.

Frontier orbitals. To experimentally determine the frontier orbitals a CV experiment was performed as presented in ESI **Fig. S2**. The oxidation onset was determined to 0.98 V affording a HOMO level of -5.23 eV. The onset of the absorbance is determined to be 898 nm yielding an optical band gap of 1.38 eV. Using the optical band gap, the LUMO level is calculated to be -3.85 eV. Stalder *et al*.[32] reported that the placement of the LUMO should be in the range of -3.8 to -4 eV, which is supported by the CV findings. The found LUMO align well (as mentioned above) to the energy level -4.03 eV of PC[60]BM, although it is generally considered that 0.3 eV is the optimal $LUMO_{ACCEPTOR}$-$LUMO_{DONOR}$ difference to ensure the highest charge separation. Even though the found difference of our system is slightly lower (0.2 eV), this is expected to still be sufficient to ensure charge separation. The LUMO of **PDTPI** is slightly higher than the LUMO found in Wu *et al.*[17] where the LUMO of a similar polymer, was determined to be -3.61 eV. The polymer Wu *et al.* is only differing from **PDTPI** with one extended thiophene on each side of the DTP moiety. Likewise the HOMO level of the similar polymer was found to be -4.94 eV, therefore the removal of the thiophene, will make the **PDTPI** more stable under ambient conditions, while still maintaining the favorable LUMO level of the *i*-ID. Comparing with the DFT simulations, the difference is rather large. This difference can be ascribed two major contributions, firstly the fact that the relative conjugation length is rather low compared to the experimental data, which in reality is approximately 11 continuously linked D-A couples. Also the spatial dimension of the polymer is neglected in the type of DFT modelling applied, this meaning that the π-π stacking of the polymers are not evaluated. Despite the mismatch with the experimental values, the DFT modelled data are very similar with the previously reported DFT data at the B3LYP level, which are in the range of 2.8-3 eV[27,31].

Photovoltaic properties. The photovoltaic properties of **PDTPI** were investigated by preparing flexible ITO-free organic solar cells in an inverted geometry with a bulk heterojunction active layer morphology consisting of **PDTPI** and PC[60]BM. Layer depositions were conducted both by spin coating and, the more industrial scale suitable, slot-die coating on a mini roll coater. The corresponding I-V curves and photovoltaic data, PCE, open circuit voltage (V_{oc}),

short circuit current (J_{sc}), and fill factor (FF), can be seen in **Fig 4.** and **Table 1**, respectively. The spin-coated devices achieved, a lower PCE (0.72%) than was reached on slot-die coated devices with the same composition. This is exclusively due to an increased J_{SC} for the slot-die coated devices. The improvement could be seen as an abnormality, since not only is the deposition method changed from spin-coating to slot-die coating; but also the area increases from 0.25 cm^2 to 1 cm^2, which would usually lead to a decreased J_{SC}. The observed increase can be explained by the utilization of a different PEDOT:PSS top-electrode where the spin-coated devices were based on Agfa EL-P5010, the roll-coated devices had the 3 layer PEDOT:PSS electrode, as seen in **Fig 1.** Meanwhile there must exist different morphology caused by different solvent evaporation rate between the roll coated and spin coated process, this would play an impact, thus result in different short-circuit density. However this is not the focus of this work, further studies on morphology effects, when going from spin coated to roll coated, could be pursued in the near future.

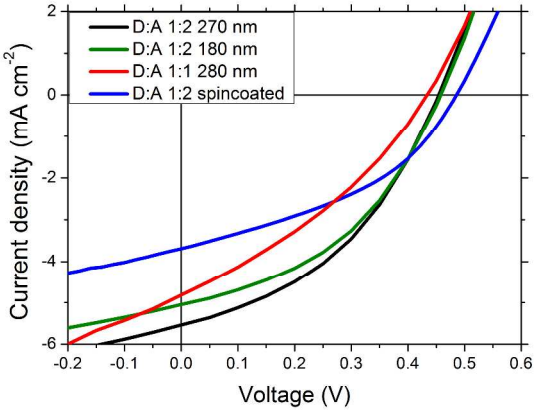

Figure 4. I-V curves of roll coated and spin coated single junction solar cells with different PDTPI/PC[60]BM ratio and film thickness. The estimated thickness of the active layer in spin coated cell (D:A 1:2) was 160-200nm.

To optimize the **PDTPI**:PC[60]BM composition two different compositions (1:1 and 1:2) were tested. The results in **Table 1** clearly reveal that the 1:2 composition is better, which besides an increase in PCE from 0.62 % to 0.99 % also improved in the remaining photovoltaic characteristics.

Table 1. Performance data of the single junction roll-coated devices

D:A	L(nm)	Voc (V)	Jsc(mA cm^{-2})	FF (%)	PCE(%)
1:1	280	0.42 ± 0.01	-4.6± 0.2	32.3 ± 0.6	0.62 ± 0.05
1:2[1]	*	0.49	-3.69	40.3	0.72
1:2	180	0.45 ± 0.004	-4.95 ± 0.18	40.9 ± 1.1	0.92 ± 0.05
1:2	270	0.46 ± 0.004	-5.25 ± 0.28	41.3 ± 1.4	0.99 ± 0.08

D: PDTPI, A: PC[60]BM, L: Thickness, [1] Spin-coated sample, * estimated active layer thickness was 160-200 nm.

Most significantly is the increase in FF with approximately 25 %, a possible explanation could be the improved interface or more likely improved carrier transport in the active layer, which together with a possible increase in exciton dissociation accounts for the increase in J_{SC} due to a reduced recombination. The film thickness was investigated by producing devices with 270 nm and 180 nm thick active layers. Reducing the film thickness resulted in a slight decrease in device efficiency due to a decrease in J_{SC} most likely due to a reduced absorption whereas the remaining photovoltaic characteristics were unaffected.

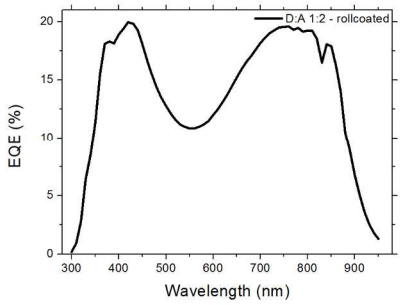

Figure 5 EQE of the best performing single junction device, of PDTPI/PC[60]BM ratio 1:2 with an active layer thickness of 280 nm

The better performing devices were therefore prepared with an active layer composition of 1:2 between **PDTPI** and PC[60]BM with a thickness of 280 nm, achieving a PCE of 0.99 %, which for J_{SC} was verified by EQE (seen in **Fig.5**) giving a J_{SC} of 5.30 mA cm^{-2} correlating nicely with the measured 5.25 mA cm^{-2}(see **Table 1**) These results does however not show the full potential of **PDTPI** since Flextrode, has a decreasing transmission from 60 % to 35 % in the interval from 600 nm to 900 nm[33] which is where **PDTPI** is photoactive (see **Fig. 2**).

The absorption characteristics of **PDTPI** which has a primary absorbing from 600-900 nm (**Fig. 2**) could make it a prime candidate for the low band gap junction in tandem solar cells. As a high band gap polymer P3HT and PBDTTTz-4 was chosen due to their ideal spectral match with **PDTPI** as shown in **Fig.6**.

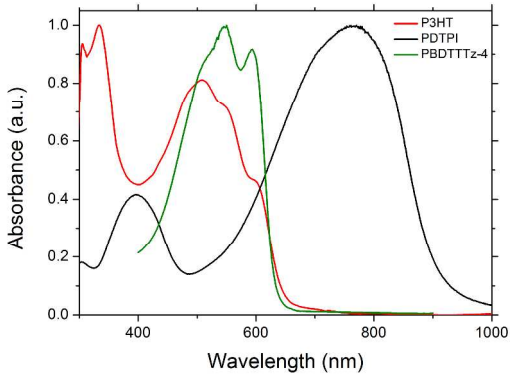

Figure 6 The film absorbance of PBDTTTz-4 (green line), PDTPI (black line) and P3HT (red line).

Tandem solar cells were prepared on the roll coater by slot-die coating and flexographic print via the method presented by Andersen *et al*.[22,34] the layer structure is shown in **Fig. 1**. Results from the three different tandem solar cells combinations prepared can be seen in **Table 2**. In **Fig. 7** the I-V characteristics of the 3 best performing devices with **PBDTTTz-4** and **P3HT** combined with **PDTPI**, respectively. It is clear that the V_{OC} is lower than the theoretically maximum estimated as the sum of the single junction V_{OC}'s. This has however been reported previously in several cases when using flexible substrates[22,35,36] in which the tandem cell open-circuit voltages are 10-15 % lower. It is clear that the tandem consisting of **PDTPI** and P3HT is under performing, due to both lower J_{SC} and FF. This is despite a close to ideal spectral overlap between **P3HT** and **PDPTI**.

Table 1. The layer composition and performance of the tandem solar cells; with PDTPI as low band gap polymer, combined with P3HT or PBDTTTz-4 as high band gap polymer, respectively.

Composition	Voc (V)	Jsc(mA cm^{-2})	FF (%)	PCE (%)	Best PCE [%]
180 nm P3HT 270 nm PDTPI	0.85± 0.01	-2.49± 0.07	35.17± 0.05	0.74± 0.01	0.75
155 nm PBDTTTz-4 350 nm PDTPI	0.95± 0.02	2.83± 0.98	33.85± 3.84	1.12± 0.23	1.40
290 nm PBDTTTz-4 350 nm PDTPI	1.08± 0.09	4.60± 0.32	32.93± 0.52	1.63± 0.05	1.73

The efficiencies obtained for the **PBDTTTz-4** and **PDTPI** combination outperformed the **P3HT**:**PDTPI** combination with similar active layers thicknesses, mostly due to an increase in V_{OC}. The effect of layer thickness of tandem devices are clear when comparing the large difference in PCE for devices prepared with front junction thicknesses of 155 nm and 290 nm. 0

The increase in V_{OC} with increasing front junction thickness is likely due to the usage of Flextrode which previously have been shown to contain rather large silver spikes[22,35]; as a larger number of spikes will be embedded in the front junction as relative to the back junction, increasing the front junction thickness will result in fewer penetrating silver spikes and hence the level of shunting will be reduced. The increase in J_{SC} can be ascribed to a better current matching between the junctions.

The best performing device showed a PCE of 1.73% and consists of a 290 nm **PBDTTTz-4** front junction and a 350 nm back junction of **PDTPI**, shown as the black line in **Fig. 7**.

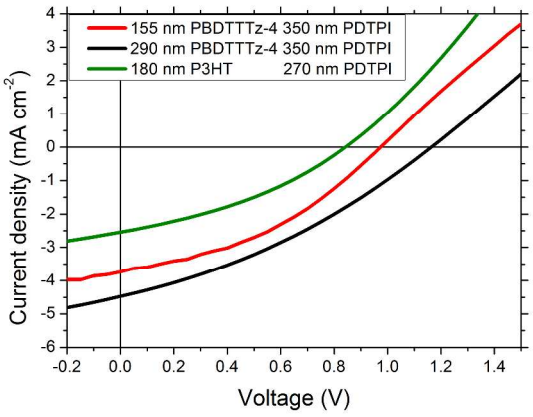

Figure 7 I-V characteristics of the tandem solar cells with the following combinations, 155 nm PBDTTTz-4 350 nm PDTPI (red line), 290 nm PDBTTTz-4 350 nm PDTPI (black line) and 180 nm P3HT 270 nm PDTPI (green line).

Conclusions

A low-band gap polymer consisting of alternating di(2-ethylhexyl)isoindigo and *N*-(1-pentylhexyl)dithieno[3,2-*b*:2',3'-*d*]-pyrrole moieties were synthesized. The synthesized polymer had a band gap of 1.38 eV with a HOMO level at -5.23 eV (determined by CV) and a suitably aligned LUMO level of -3.85 eV; which makes it an ideal donor for the PC[60]BM. Density function theory (DFT) computations showed, that the LUMO was primarily located on the acceptor while the HOMO likewise was distributed on the donor moiety, *i*-ID and DTP, respectively. The DFT simulations also showed a torsion angle between the donor and acceptor moiety at around 22°, this combined with a simulation of an extended D-A structure showed a continuous torsion. This torsion could explain the relative small onset redshift (~25 nm) in absorbance when going from solution to film. Large area (0.25 to 1 cm^2), ITO-free single junction photovoltaics showed efficiencies ranging from 0.72 % to 0.99 % for spin-coated and roll-coated, respectively. The low band gap and the EQE characteristics of **PDTPI** combined with the nice spectral overlap with PBDTTTz-4 and P3HT made it an ideal candidate for a back cell in a tandem solar cell. Large area (0.8 cm^2), ITO-free roll-coated tandem junction photovoltaics were produced with efficiencies ranging 0.72 % to 1.72 %, for **PDTPI** combined with P3HT and PBDTTTz-4, respectively.

Acknowledgements

The authors would like to gratefully acknowledge the financial support from the Danish Council for Strategic Research through the WAPART project (Water-based particulate approach to organic photovoltaics with controlled morphology, 11-116380), and the Danish National Research Foundation (DNRF) for the Danish-Chinese Center for Organic based Photovoltaic Cells with Morphological Control. Support from the Sino-Danish Centre for Education and Research (SDC) is also fully acknowledged.

Notes and references

[a] Department of Chemistry and Bioscience, Aalborg University, Fredrik Bajers Vej 7H, DK-9220, Aalborg East, Denmark
[b]Sino-Danish Centre for Education and Research (SDC), Niels Jenses Vej 2, DK-8000, Aarhus, Denmark
[c] Department of Energy Conversion and Storage, Technical University of Denmark, Frederiksborgvej 399, DK-4000, Roskilde, Denmark
[d]Department of Engineering, Aarhus University, Hangoevej 2, 8200 Aarhus N, Denmark
* Corresponding authors: yu@bio.aau.dk
† Equal contributions to this work
Electronic Supplementary Information (ESI) available: [details of any supplementary information available should be included here]. See DOI: 10.1039/c000000x/

1. H. Xin, X. Guo, F. S. Kim, G. Ren, M. D. Watson and S. A. Jenekhe, *J. Mater. Chem.*, 2009, **19**, 5303-5310.
2. X. Guo, F. S. Kim, M. J. Seger, S. A. Jenekhe and M. D. Watson, *Chem. Mater.*, 2012, **24**, 1434–1442.
3. X. Zhan, Z. Tan, E. Zhou, Y. Li, R. Misra, A. Grant, B. Domercq, X.-H. Zhang, Z. An, X. Zhang, S. Barlow, B. Kippelen and S. R. Marder, *J. Mater. Chem.*, 2009, **19**, 5794-5803.
4. B. a. D. Neto, A. a. M. Lapis, E. N. da Silva Júnior and J. Dupont, *European J. Org. Chem.*, 2013, 228–255.
5. S. Qu and H. Tian, *Chem. Commun. (Camb).*, 2012, **48**, 3039–3051.
6. W. Yue, X. Huang, J. Yuan, W. Ma, F. C. Krebs and D. Yu, *J. Mater. Chem. A*, 2013, **1**, 10116-101119.
7. B. R. Aïch, S. Beaupré, M. Leclerc and Y. Tao, *Org. Electron.*, 2014, **15**, 543–548.
8. R. Stalder, J. Mei and J. R. Reynolds, *Macromolecules*, 2010, **43**, 8348–8352.
9. E. Bundgaard and F. Krebs, *Sol. Energy Mater. Sol. Cells*, 2007, **91**, 954–985.
10. J.-L. Brédas, D. Beljonne, V. Coropceanu and J. Cornil, *Chem. Rev.*, 2004, **104**, 4971–5004.
11. J. Mei, K. R. Graham, R. Stalder and J. R. Reynolds, *Org. Lett.*, 2010, **12**, 660–663.
12. G. Zhang, Y. Fu, Z. Xie and Q. Zhang, *Macromolecules*, 2011, **44**, 1414–1420.
13. B. Liu, Y. Zou, B. Peng, B. Zhao, K. Huang, Y. He and C. Pan, *Polym. Chem.*, 2011, **2**, 1156-1162.
14. E. Wang, Z. Ma, Z. Zhang, P. Henriksson, O. Inganäs, F. Zhang and M. R. Andersson, *Chem. Commun. (Camb).*, 2011, **47**, 4908–4910.
15. E. Wang, Z. Ma, Z. Zhang, K. Vandewal, P. Henriksson, O. Inganäs, F. Zhang and M. R. Andersson, *J. Am. Chem. Soc.*, 2011, **133**, 14244–14247.
16. Y. Deng, J. Liu, J. Wang, L. Liu, W. Li, H. Tian, X. Zhang, Z. Xie, Y. Geng and F. Wang, *Adv. Mater.*, 2014, **26**, 471–476.
17. F. Wu, H. Yang, C. M. Li and J. Qin, *Polym. Adv. Technol.*, 2013, **24**, 945–950.
18. F. C. Krebs, *Sol. Energy Mater. Sol. Cells*, 2009, **93**, 1636–1641.
19. F. C. Krebs, *Org. Electron.*, 2009, **10**, 761–768.
20. W. Yue, T. T. Larsen-Olsen, X. Hu, M. Shi, H. Chen, M. Hinge, P. Fojan, F. C. Krebs and D. Yu, *J. Mater. Chem. A*, 2013, **1**, 1785-1793.
21. D. Angmo, S. a. Gevorgyan, T. T. Larsen-Olsen, R. R. Søndergaard, M. Hösel, M. Jørgensen, R. Gupta, G. U. Kulkarni and F. C. Krebs, *Org. Electron.*, 2013, **14**, 984–994.
22. T. R. Andersen, H. F. Dam, B. Andreasen, M. Hösel, M. V. Madsen, S. a. Gevorgyan, R. R. Søndergaard, M. Jørgensen and F. C. Krebs, *Sol. Energy Mater. Sol. Cells*, 2014, **120**, 735–743.
23. M. M. Wienk, M. Turbiez, J. Gilot and R. A. J. Janssen, *Adv. Mater.*, 2008, **20**, 2556–2560.
24. R. C. Coffin, J. Peet, J. Rogers and G. C. Bazan, *Nat. Chem.*, 2009, **1**, 657–661.
25. C.-C. Ho, S.-Y. Chang, T.-C. Huang, C.-A. Chen, H.-C. Liao, Y.-F. Chen and W.-F. Su, *Polym. Chem.*, 2013, **4**, 5351-5360.
26. R. Stalder, C. Grand, J. Subbiah, F. So and J. R. Reynolds, *Polym. Chem.*, 2012, **3**, 89-92.
27. P. Salvatori, E. Mosconi, E. Wang, M. Andersson, M. Muccini and F. De Angelis, *J. Phys. Chem. C*, 2013, **117**, 17940–17954.
28. S. Zhang, H. Fan, Y. Liu, G. Zhao, Q. Li, Y. Li and X. Zhan, *J. Polym. Sci. Part A Polym. Chem.*, 2009, **47**, 2843–2852.
29. T. Lei, J.-H. Dou, Z.-J. Ma, C.-H. Yao, C.-J. Liu, J.-Y. Wang and J. Pei, *J. Am. Chem. Soc.*, 2012, **134**, 20025–20028.
30. Z. Wang, J. Zhao, Y. Li and Q. Peng, *Polym. Chem.*, 2014, **5**, 4984-4992.
31. W. Zhuang, M. Bolognesi, M. Seri, P. Henriksson, D. Gedefaw, R. Kroon, M. Jarvid, A. Lundin, E. Wang, M. Muccini and M. R. Andersson, *Macromolecules*, 2013, **46**, 8488–8499.
32. R. Stalder, J. Mei, K. R. Graham, L. A. Estrada and J. R. Reynolds, *Chem. Mater.*, 2014, **26**, 664–678.
33. M. Hösel, R. R. Søndergaard, M. Jørgensen and F. C. Krebs, *Energy Technol.*, 2013, **1**, 102–107.
34. T. R. Andersen, H. F. Dam, M. Hösel, M. Helgesen, J. E. Carlé, T. T. Larsen-Olsen, S. a. Gevorgyan, J. W. Andreasen, J. Adams, N. Li, F. Machui, G. D. Spyropoulos, T. Ameri, N. Lemaître, M. Legros, A. Scheel, D. Gaiser, K. Kreul, S. Berny, O. R. Lozman, S. Nordman, M. Välimäki, M. Vilkman, R. R. Søndergaard, M. Jørgensen, C. J. Brabec and F. C. Krebs, *Energy Environ. Sci.*, 2014, **7**, 2925-2933.
35. T. R. Andersen, H. F. Dam, B. Burkhart, D. Angmo, M. Corazza, B. C. Thompson and F. C. Krebs, *J. Mater. Chem. C*, 2014, **2**, 9412–9415.
36. N. Li, D. Baran, G. D. Spyropoulos, H. Zhang, S. Berny, M. Turbiez, T. Ameri, F. C. Krebs and C. J. Brabec, *Adv. Energy Mater.*, 2014, **4**, 1400084.
37. M. Zhang, Y. Sun, X. Guo, C. Cui, Y. He and Y. Li, *Macromolecules*, 2011, **44**, 7625–7631.
38. M. Helgesen, J. E. Carle and F. C. Krebs, *Adv. Energy Mater.*, 2013, **3**, 1664-1669

Table of Contents Graph for

An isoindigo containing donor-acceptor polymer: synthesis and photovoltaic properties of all-solution-processed ITO- and vacuum-free large area roll-coated single junction and tandem solar cells

Rasmus Guldbaek Brandt [a,b,†], Wei Yue [a,b,†], Thomas Rieks Andersen [c], Thue Trofod Larsen-Olsen [c], Mogens Hinge [d], Eva Bundgaard [c], Frederik C. Krebs [c], Donghong Yu [a,*]

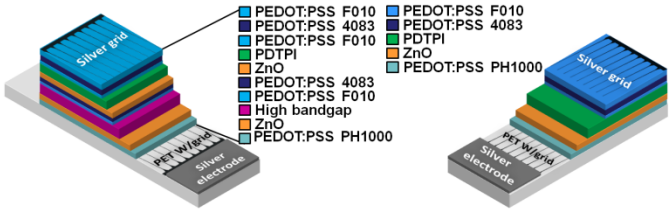

Novel donor-acceptor polymer from isoindigo and dithieno[3,2-b:2',3'-d]-pyrrole were developed for large area ITO-free via a fully roll-coated devices both as single junction (1 cm^2) and tandem solar cells (0.8 cm^2), they showed excellent scalability, with little efficiency loss going from the 0.25 cm^2 spin coated device to the 1 cm^2 roll coated device.